Azimuthal reflectivity inversion

Jon Downton
CGGVeritas
Jon.Downton@cggveritas.com

Benjamin Roure
CGGVeritas
Benjamin.Roure@cggveritas.com

Olivia Collet *
CGGVeritas
Olivia.Collet@cggveritas.com

Loic Michel
CGGVeritas
Loic.Michel@cggveritas.com

SUMMARY

Seismic fracture prediction is becoming a more important exploration and development problem with the growing focus on unconventional reservoirs. A non-linear inversion technique is presented to estimate layer-based fracture parameters and velocities based on azimuthal reflectivity data. The earth model assumes a single set of vertical fractures per layer parameterized in terms of linear slip parameters - the normal and tangential fracture weaknesses - and fracture strike. In addition, the background P-wave and S-wave impedances are estimated. Either the exact Zoeppritz equation or some linearization thereof is used in a convolutional modelling scheme to estimate seismic amplitude data. The inverse problem is solved in a nonlinear fashion using simulated annealing.

The new technique has several advantages over performing azimuthal amplitude versus angle analysis (AVAz). The reflectivity calculation used in the new technique is more theoretically correct, allowing for the symmetry plane to change as a function of layer. The 90 degree ambiguity in estimating the symmetry plane typical of the near offset approximation also disappears. Further, there is an improvement in the isotropic parameter estimates compared to isotropic inversion since the bias introduced by neglecting anisotropy has been removed by incorporating it into the forward model. The azimuthal inversion is demonstrated on both synthetic and real seismic data.

Key words: inversion, azimuthal, anisotropy, fracture, reservoir.

INTRODUCTION

The estimation of HTI anisotropy has proved useful to predict fractures (Hunt *et al.*, 2010) and horizontal stress (Gray, 2010). One proven method to predict HTI anisotropy is azimuthal AVO. Rüger (2002) derived a linearized approximation to the Zoeppritz equation for HTI anisotropy. The near offset approximation of this is similar to the two-term Shuey's AVO equation with two extra parameters, the anisotropic gradient and the symmetry plane. For fractured media, the anisotropic gradient is often claimed to be proportional to crack density while the isotropy plane is thought to be the strike of the fractures. There are a number of assumptions and limitations with this theory. First, the derivation assumes an isotropic half-space over an anisotropic half-space. This assumption is restrictive as we would like to generalize the model to the case of a stack of anisotropic layers. Secondly, as Goodway *et al.* (2006) argue, the near offset approximation is susceptible to theoretical error introduced by the far offset terms. In addition, the anisotropic gradient is actually a function of Thomsen's anisotropic parameters delta and gamma. These two parameters may not be correlated in the same fashion to crack density giving rise to a potentially complex relation between crack density and the anisotropic gradient. Furthermore, there is a 90 degree ambiguity associated in the estimatation of the isotropy plane. Lastly the azimuthal AVO inversion estimates only fractional band-limited elastic parameters. Simultaneous prestack elastic inversion is one way to address these limitations. Coulon et al. (2006) demonstrated a simultaneous prestack inversion to invert for isotropic elastic parameters using a simulated annealing algorithm. This paper extends this approach to anisotropic media and by so doing addresses the limitations outlined above. This paper first reviews the 3D, simultaneous isotropic elastic inversion of Coulon *et al.* (2006). The isotropic simultaneous inversion uses a 1D convolutional modelling scheme where the reflectivity is modelled by the Zoeppritz equation or a linear approximation. There is then a discussion about how the reflectivity modelling is generalized to the case of two orthorhombic half-spaces with arbitrary rotated symmetry planes following Schoenberg and Protázio (1992). Even though the reflectivity modelling supports orthorhombic anisotropy, the more restricted case of HTI anisotropy is assumed to reduce the number of free parameters solved for. Moreover, alternative parameterizations incorporating fractured rock physics, such as the penny-shaped crack model (Hudson *et al.*, 1981) or linear slip deformation theory (Schoenberg and Sayers, 1995) are explored. After describing the calculation and parameterization of the anisotropic Zoeppritz equation, the generalization of the Coulon *et al.* (2006) method to anisotropic media is described. The method is then demonstrated on both synthetic and real data.

THEORY

Coulon *et al.* (2006) describe a 3D multi-cube simultaneous isotropic elastic inversion. The inversion is 3D in the sense that it solves for 3D volumes of elastic parameters and incorporates multi-trace lateral continuity constraints in the objective function. Nevertheless, the data are modelled using a 1D convolutional approach. The reflectivity is modelled using the full Zoeppritz equation or a linearized version thereof. The inputs to the algorithm are angle stacks and some initial layered elastic model defined in the time domain. By using angle stacks, NMO stretch (Roy *et al.*, 2005) and scaling issues can be addressed by varying the wavelet as a function of angle of incidence. Further, ray tracing need not be performed, simplifying the forward modelling. The initial model is iteratively perturbed using simulated annealing to find a global solution which minimizes the objective function. The objective function contains a data misfit and

regularization term. The regularization term includes a 3D spatial continuity constraint to help attenuate the effects of random noise. Further, since the algorithm is nonlinear, bounds may be easily incorporated. The algorithm perturbs the layer P-wave velocity, V_p, S-wave velocity, V_s, and density, ρ. These parameters can be perturbed independently or coupled via relationships such as the Gardner's relation linking V_p and ρ. In addition to the elastic parameters, the method also perturbs the time-thickness of the micro-layers so as to reduce the data misfit and enhance lateral coherence.

Extension of simultaneous inversion: from isotropy to anisotropy

The reflectivity calculation needs to be modified to incorporate HTI anisotropic media. The HTI layered medium may be parameterized in terms of the layer time-thickness, P-wave and S-wave impedances, density, and the Thomsen parameters δ, ε and γ, and the azimuth of the isotropy plane. This gives 8 free parameters per layer. The HTI stiffness matrix is calculated from the elastic parameters defining each layer. Next, the isotropy plane information is used to perform a Bond transformation (Winterstein, 1990). This formulation allows the isotropy plane to vary as a function of layer or equivalently depth. Schoenberg and Protázio (1992) solve for the Zoeppritz reflectivity using the rotated stiffness matrices as input. The reflectivity is modelled for each interface resulting in a reflectivity series. This reflectivity series is then convolved with a user-defined wavelet to create a model of the data for a particular azimuth and angle of incidence. The simultaneous inversion methodology of Coulon et al. (2006) using simulated annealing extends naturally to the nonlinear forward modelling described above.

Fracture parameters

HTI anisotropy introduces four additional parameters compared to the four parameters of the isotropic inverse problem (i.e. three Thomsen parameters and the azimuth of the isotropy plane). This raises the question whether the problem is well enough posed to obtain a reliable estimate of all these parameters. It is possible to reduce the number of free parameters by using rock physics models. The linear slip theory of Schoenberg and Sayers (1995) reduces the number of parameters describing the HTI stiffness matrix by one. In this theory, the stiffness matrix is described by the isotropic parameters λ and μ, and the normal and tangential weaknesses, Δ_N and Δ_T. These weakness parameters describe how fractures weaken a background isotropic rock resulting in the density normalized stiffness matrix

$$\mathbf{A}=\begin{pmatrix} \frac{M}{\rho}(1-\Delta_N) & \frac{\lambda}{\rho}(1-\Delta_N) & \frac{\lambda}{\rho}(1-\Delta_N) & 0 & 0 & 0 \\ \frac{\lambda}{\rho}(1-\Delta_N) & \frac{M}{\rho}(1-\chi^2\Delta_N) & \frac{\lambda}{\rho}(1-\chi\Delta_N) & 0 & 0 & 0 \\ \frac{\lambda}{\rho}(1-\Delta_N) & \frac{\lambda}{\rho}(1-\chi\Delta_N) & \frac{M}{\rho}(1-\chi^2\Delta_N) & 0 & 0 & 0 \\ 0 & 0 & 0 & \frac{\mu}{\rho} & 0 & 0 \\ 0 & 0 & 0 & 0 & \frac{\mu}{\rho}(1-\Delta_T) & 0 \\ 0 & 0 & 0 & 0 & 0 & \frac{\mu}{\rho}(1-\Delta_T) \end{pmatrix}$$

where $\chi = \lambda/M = 1-2g$, with $M=\lambda+2\mu$ and g equal to the square of the background S-wave to P-wave velocity ratio for the unfractured rock. Both the normal and tangential weakness parameters are bound between 0 and 1.

The introduction of fractures (positive normal and tangential weaknesses) reduces both the P-wave and S_V-wave velocities in the symmetry plane (square root of A_{11} and A_{55} terms respectively). In contrast the S_V-wave velocity in the isotropy plane (square root of A_{44} term) is uninfluenced by the fractures. Since χ is typically small, the P-wave velocity (square root of A_{33} term) in the isotropy plane is also largely uninfluenced.

The penny-shaped crack model of Hudson *et al.* (1981) provides an alternative way to parameterize the model space in terms of ξ, the crack density, and ς, which is related to the fluid compressibility and the fracture aperture. If the fluid is known a priori to be gas, such as in the Western Canadian Deep Basin, the unknown anisotropic parameters can be reduced to just the crack density and isotropy plane azimuth. The penny-shaped crack model creates a coupling between the normal and tangential weaknesses limiting the solution space. Interestingly the tangential weakness is only a function of crack density while the normal weakness is also a function of the fluid elastic properties. These parameters complement the λρ, μρ methodology of Goodway *et al.* (1997).

Consequently, the density normalized HTI stiffness matrix may be calculated by one of these methods for each layer. After the parameterization is performed for a particular layer and location, the stiffness matrix is rotated so that the isotropy plane is parallel to the fracture strike. The Bond transformation allows the isotropy plane to vary as a function of layer. The reflectivity, or reflection coefficient, is then calculated using the anisotropic Zoeppritz equation or linearization thereof. The reflectivity is calculated for each azimuth, angle of incidence, and interface. Accordingly, each azimuth and angle of incidence has a reflectivity series, which, when convolved with a wavelet, represents a synthetic seismic trace.

Having extended the forward modelling to anisotropic media and developed suitable parameterizations, it is now possible to describe how the simultaneous inversion methodology of Coulon *et al.* (2006) is extended to anisotropic media. The inputs to the algorithm are still angles stacks but now specified at a variety of different azimuths. For example, in the real data example shown in the next section, four angle stacks are used and six azimuths (i.e. 15, 45, 75, 105, 135 and 165 degrees) resulting in 24 input cubes for the inversion. The input angle-azimuth stacks are created using a controlled amplitude processing flow outlined by Gray *et al.* (2009). In addition to the isotropic initial layered model, the user must also specify the anisotropic model. In the absence of knowledge, the initial model is typically assumed to be isotropic.

The simultaneous inversion is similar to the isotropic inversion but with the incorporation of azimuthal effects. The initial model is iteratively perturbed using a simulated annealing algorithm to minimize the objective function. The data misfit portion of the objective function minimizes the differences between the anisotropic forward modelling described above and the angle-azimuth amplitude cubes. The regularization term in the objective function once again optimizes 3D spatial continuity. The perturbations may be applied to individual parameters or perturbations can be coupled via correlations between the parameters. Both the linear slip theory and Hudson parameterizations couple Thomsen parameters and limit the solution space.

RESULTS

The algorithm was tested on both real and synthetic data. Table 1 shows the parameters used to generate synthetic data for two tests that were performed. Each layer is 50ms thick. Both the second and third layers are anisotropic with different symmetry planes. This case breaks the assumptions made by the Rüger's (2002) equation. The data were forward modelled using the anisotropic Zoeppritz equation generating reflectivity for angle of incidence stacks at 10, 20, 30 and 40 degrees and for azimuths at 0, 30, 60, 90, 120, and 150 degrees. These angle-azimuth stacks were then convolved with an 80Hz Ricker wavelet. Data were generated for a 3D volume with laterally invariant parameters. The noise-free synthetic seismic data were then inverted using the simultaneous anisotropic inversion. Figure 3 shows the anisotropic parameter estimates displayed as probability distribution functions (PDF). The ideal solution is highlighted with red lines. The match is excellent with only a small amount of scatter about the ideal solution. The robustness to noise was also studied and provided good results.

Layer	Vp (m/s)	Vs (m/s)	ρ (g/cm^3)	Δ_N	Δ_T	Φ_{sym} (°)
1	2647	1180	2.1	0	0	0
2 (HTI)	3641	2010	2.4	0.3	0.1	45 or 135
3 (HTI)	3641	2010	2.4	0.1	0.3	90
4	2647	1180	2.1	0	0	0

Table 1: Input models used to generate the synthetic seismic data. Two different models were generated: one with the second layer having a 45° symmetry axis Φ_{sym} and the other with the second layer having a 135° symmetry axis Φ_{sym}.

Table 1 shows two different models for the second layer, one with a 45° symmetry axis and the other with a 135° symmetry axis. This was done to test whether the algorithm resolved the 90° symmetry plane ambiguity that the near offset Rüger's (2002) equation has. The inversion gave correct results in both cases.

The inversion was applied on a 3D seismic dataset from North-Eastern British Columbia. The corresponding estimates of the normal and tangential weaknesses Δ_N and Δ_T and the symmetry axis Φ_{sym} are shown in Figure 4. Recall that in fractured media the tangential weakness is proportional to the crack density while the normal weakness is also a function of the crack aperture and fluid. The results are consistent with the knowledge in the field.

CONCLUSIONS

In summary, we have developed and demonstrated a new 3D simultaneous elastic inversion for HTI anisotropic media. The method is an extension of the isotropic simultaneous inversion of Coulon *et al.* (2006). The method addresses a number of theoretical shortcomings of azimuthal AVO. Rather than producing fractional elastic parameter estimates, the inversion produces elastic parameter estimates. The method is general enough to allow each layer to be HTI anisotropic with an arbitrary rotation for the symmetry axis. The forward modelling calculates the reflectivity using the anisotropic Zoeppritz equation or some linearization of this and does not rely on some near offset approximation to enhance stability. Lastly, the 90° symmetry axis ambiguity has been removed. The algorithm was demonstrated on both synthetic and real data with good results.

ACKNOWLEDGMENTS

The authors thank Philippe Doyen (CGGVeritas), Dave Gray (Nexen), Bill Goodway (Apache), Marco Perez (Apache), Daria Pusic (Encana) and Doug Anderson (Encana) for valuable discussions.

REFERENCES

Coulon, J.-P., Lafet, Y., Deschizeaux, B., Doyen, P.M., and Duboz, P., 2006, Stratigraphic elastic inversion for seismic lithology discrimination in a turbiditic reservoir: 76th Annual International Meeting, SEG, Expanded Abstracts, 25, no. 1, 2092-2096.

Goodway, B., Chen, T., and Downton, J., 1997, Improved AVO fluid detection and lithology discrimination using Lamé petrophysical parameters; "λρ","μρ",&"λ/μ fluid stack", from P and S inversions: 67th Annual International Meeting, SEG, Expanded Abstracts, 16, 183.

Goodway, B., J. Varsek, and C. Abaco, 2006, Practical applications of P-wave AVO for unconventional gas resource plays: CSEG Recorder, 31, no. 4, 52–65.

Gray, D., Schmidt, D., Nagarajappa, P., Ursenbach, C., and Downton, J., 2009, CACP azimuthal processing: CSPG CSEG CWLS joint convention.

Gray, D., Anderson, P., Logel, J., Delbecq, F., and Schmidt, D., 2010, Principle stress estimation in shale plays using 3D seismic : GeoCanada.

Hudson, J. A., 1981, Wave speeds and attenuation of elastic waves in material containing cracks: Geophysical Journal of the Royal Astronomical Society, 64, 133–150.

Hunt, L., Reynolds, S., Brown, T., Hadley, S., Downton, J., and Chopra, S., 2010, Am I really predicting natural fractures in the tight Nordegg gas sandstone of West Central Alberta: GeoCanada.

Roy, B., Anno, P., Baumel, R., and Durrani, J., 2005, Analytic correction for wavelet stretch due to imaging: SEG Convention, AVO 2.1, 234-237.

Rüger, A., 2002, Reflection coefficients and azimuthal AVO Analysis in anisotropic media, SEG geophysical monograph series number 10: SEG.

Schoenberg, M., and Protázio, J., 1992, 'Zoeppritz' rationalized and generalized to anisotropy: Journal of Seismic Exploration, 1, 125–144.

Schoenberg, M., and Sayers, C., 1995, Seismic anisotropy of fractured rock: Geophysics, 60, 204–211.

Winterstein , D. F., 1990, Velocity anisotropy terminology for geophysicists: Geophysics, 55, 1070–1088.

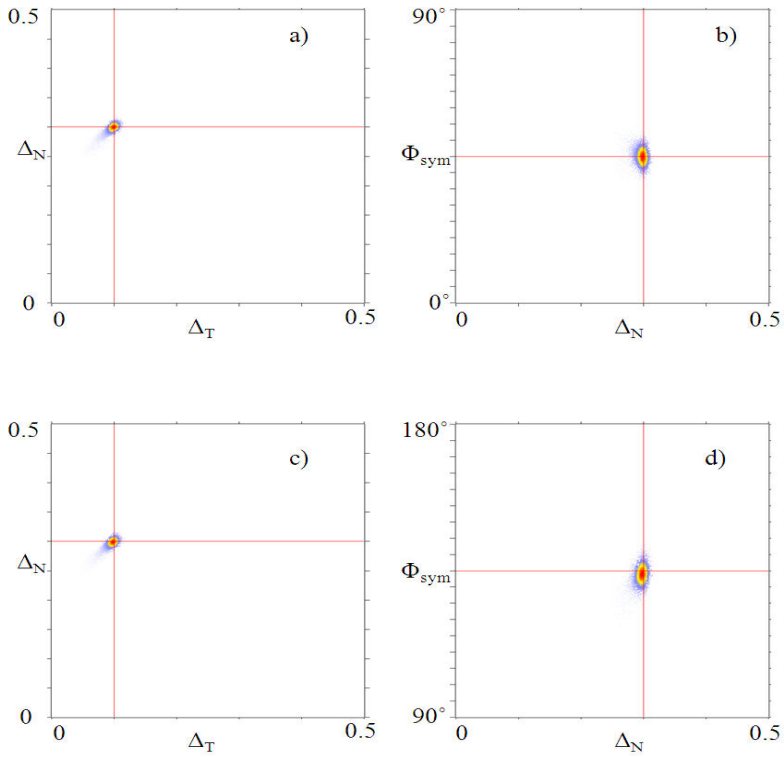

Figure 3: Cross-plots showing the second layer parameter estimates for normal weakness Δ_N, tangential weaknesses Δ_T and the symmetry axis Φ_{svm}. The 3D solution space is projected for the first model (45° symmetry axis) in the 2D spaces a) (Δ_T, Δ_N) and b) (Δ_N, Φ_{svm}) and for the second model (135° symmetry axis) in the 2D spaces c) (Δ_T, Δ_N) and d) (Δ_N, Φ_{svm}).

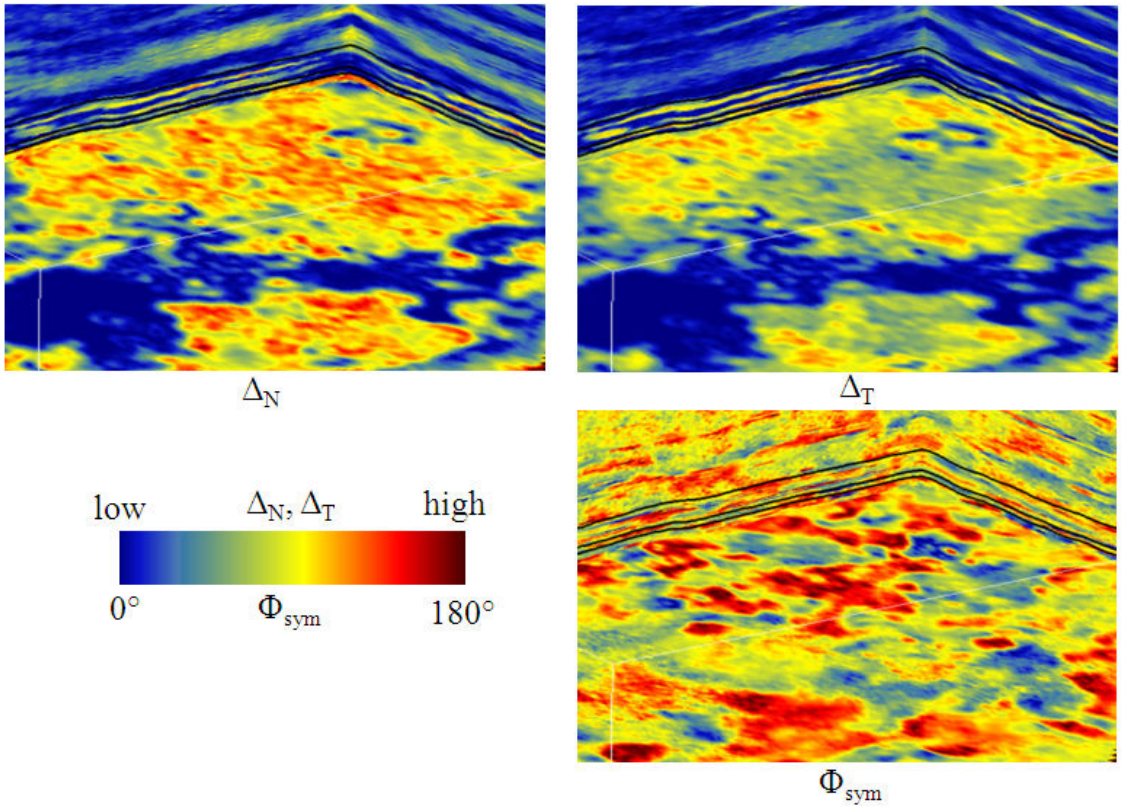

Figure 4: The estimates of the normal weakness Δ_N (top left), tangential weaknesses Δ_T (top right) and the symmetry axis Φ_{sym} (bottom right) for the real seismic data.